scientific reports

Check for updates

OPEN

Design of a novel high-sensitive SOI-Junctionless BioFET overcoming sensitivity degradation problems

Mohammad K. Anvarifard[1]✉ & Ali A. Orouji[2]

For the first time, a new configuration of label-free junctionless semiconductor device is proposed to boost sensitivity in the identification of biomolecule specifies. Instead of creating the nanocavity inside the gate oxide, the nanocavity is created in the channel region which is very useful for the SOI junctionless technology based biodevice having a high current in all operating modes. For better control of the conduction mechanism, a hole trench is created under the channel region just inside the buried oxide. This will help to modulate the energy bands terminating in enhancing the sensing performance. Unlike the conventional biosensors needing a large-scale gate oxide thickness for trapping the biomolecules, the proposed biosensor can work for very low gate oxide thickness. The different biomolecules such as Biotin, Protein A, Bacteriophage T7, and Apomyoglobin have been utilized as targeted biomolecules for evaluating the sensitivity. Comparing the proposed biosensor with the conventional and other biosensors showed an enhanced sensing performance. Practical related issues during the process of sensing in terms of fill factor percentage, steric hindrance of biomolecules, and the charges of biomolecules have been focused in the recommended biodevice. All the results exhibited high superiority of performance of the suggested biodevice as compared to the conventional biosensor.

Keywords Biosensor, Recessed nanocavity, Hole trench, Energy band modulation, Junctionless, Sensitivity

The biosensor is an electrical device to report the presence or activity of analytes utilizing a biomolecular component to bind by the target biomolecule making a detectable variation on mass, fluorescence, electric charge, refractive index. A transducer device has ability to convert these variations to the current or voltage. The biosensors are applied in many fields such as food industry, medical domain, marine section and so on[1]. Regarding the application of the biosensors in food processing, monitoring, food authenticity, quality and safety, they are used in the detection of pathogens in food, in the dairy industry and the detection and quantification of artificial sweeteners. The other applications are in the fermentation processes and ion exchange retrieval, where detection of change of biochemical composition is carried out. Also, they are prone to detect the toxicity in the foods. Regarding the application of the biosensors in the medical domain, the biosensors are broadly utilized for the diagnosis of diabetes needing the precise control of the blood glucose level. Also, they are the excellent for the identification of the infectious diseases and heat failure. Other applications are controlling endothelin-induced cardiac hypertrophy and cancer and drug exploration. It is worth noting that the application of the biosensors are not limited to the aforementioned statements, but they can be applied in the domains including the assessment of neural activities, monitoring the air quality, biodefence, the identification of the DNA strands, metabolic engineering and plant biology[1].

Nowadays, field-effect-transistor (FET) oriented biodevices have gained a high interest in the identification of biomolecules in biomedical applications owing to enhanced sensing performance with respect to other candidates. Also, the factors in terms of high scalability, low power use, and low-cost mass generation are a vital role on emphasizing the FET based biosensors[2,3].

Since the common FET based biosensors come from opposite-type doping configurations in the channel region and active area region, the creation of a scaled biosensor is very complicated due to the charge diffusion

[1]Department of Engineering Sciences, Faculty of Technology and Engineering, East of Guilan, University of Guilan, Rudsar-Vajargah, Iran. [2]Department of Electrical and Computer Engineering, Semnan University, Semnan, Iran. ✉email: m.anvarifard@guilan.ac.ir

occurring during the thermal processing of the biosensor[4,5]. A junctionless device is proposed to solve this problem by including uniform channel region with the same doping type and levels enhancing the reliability of the device and ON current, simultaneously[6,7].

Although the junctionless is a proper candidate, but it needs a double gate configuration to deplete the channel region resulting in the decreasing the OFF current. In order to solve this complexity, the Silicon-On-Insulator (SOI) technology has been proposed to reach enhanced electrical performance since it is compatible with conventional CMOS fabrication schemes and is also led to improvement of the short channel effects[8–11].

Dielectric modulated based FET biosensors (DMFET) are excellent representatives for the detection of biomolecules since they do not need the labeling process[12]. Indeed, these types of biosensors are stated as label-free biosensors giving a highly sensitive biosensor with a very low response time[13,14]. Regarding the DMFET based biosensors, a part of the gate oxide is etched leaving a nanocavity on the channel region for trapping the targeted biomolecules. Since the gate oxide is utilized to create the nanocavity, hence it is not impossible to scale the gate oxide to reach high electrical performance due to the physical limitation of probes and targeted biomolecules lengths inside the nanocavity. Therefore, a nanocavity thickness (gate oxide) of more than 5 nm is required.

In order to utilize the advantages of the SOI technology and junctionless based transistors along with keeping the scalability benefits, in this report an interesting modification has been performed on the biosensor by transferring the nanocavity from the gate dielectric to the channel region. Indeed, a nanocavity is recessed to the channel region. This architecture will provide a reduced effective silicon thickness to decrease the subthreshold current and subthreshold swing. In order to more increase the gate control on the channel region, a hole trench is created inside the buried oxide of the proposed biosensor since it helps the conduction mechanism by modulating the energy bands[15]. The stated ideas have a vital role in boosting the sensitivity and reliability of the proposed biodevice. Indeed, for the first time, a new configuration of label-free DMFET based biosensors is proposed having more desirable sensing performance than the common free-label DMFET biosensors while keeping the scalability benefits of the devices.

Recently, the novel biosensors by configuration of planar junctionless and the tunneling FET benefiting from the concept of dual material gate and charge plasma have been proposed[16–18]. The verification has been performed by the simulation analysis. Also, in the other report a novel computational framework for the evaluation of the biosensors has been presented[19].

Configuration of proposed biosensor

In this section a three-dimensional (3D) view of the novel configuration of junctionless FET biodevice is depicted according in Fig. 1. Regarding the figure, there is a fundamental change in the configuration of the conventional junctionless biosensor. The nanocavity which is the most important part for the detection of the biomolecules has

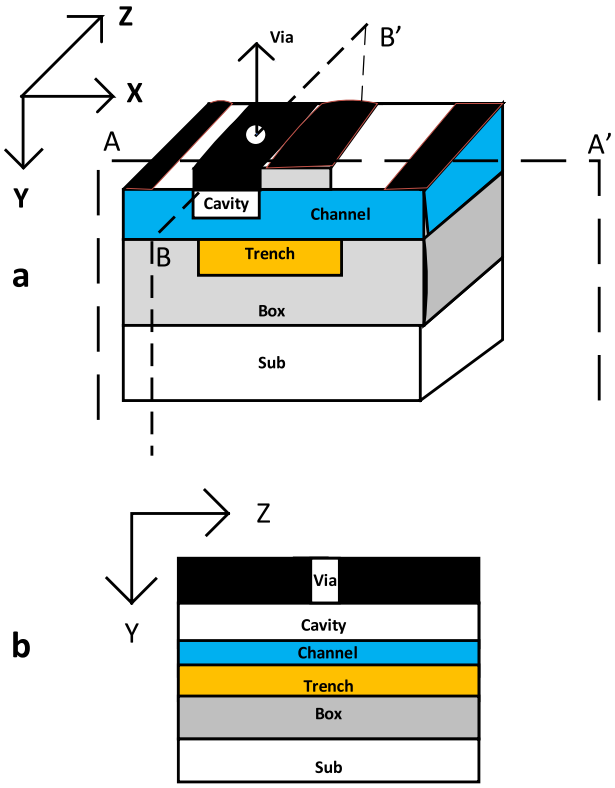

Figure 1. (**a**) The Three-dimensional (3D) proposed biosensor view (**b**) two-dimensional (2D) view along plane BB'.

been embedded in the charnel region not in the gate oxide. This is a useful work since it does not involve the gate oxide, directly. Two important conclusions can be obtained from this work. The first one is that the realization of thinner gate oxide can increase the gate control on the channel region thus enhancing the sensitivity of the biodevice owing to the reduced subthreshold swing. Because of the limitation on the nanocavity thickness, it is not possible for the CJNL. The second one is the reduced channel region thickness to reduce the subthreshold current thus enhancing sensitivity.

For better control of the channel electrostatic, a hole trench is inserted beneath the channel region inside the buried oxide. The appearance of a depletion film in the channel region/buried oxide interface is caused by this operation. Hence, the subthreshold swing is reduced thus increasing the sensitivity. Owing to inserting the hole trench and configuration of recessed nanocavity, the proposed junctionless biodevice has been called an HTRN-JNL biosensor in this paper. For more clarification a two-dimensional (2D) view of the proposed biosensor along the plane BB' has been shown. Regarding the figure, the biomolecule is injected in the nanocavity by creating a via in the gate electrode. In order to settle the biomolecule, the biosensor is completely immerged in a buffer solution including targeted biomolecules. Then the device is dried by the Argon plasma including[20] . Also, the microfluid device can be used to inject the biomolecule inside the nanocavity through the created via.

The Two-dimensional (2D) simulator involving the fundamental equations has been used to solve the equations in lattice grids created in the proposed biosensor perspective along plane AA' as shown in Fig. 2. For more specification, the conventional junctionless FET biosensor (CJNL) has been attached to the figure.

Regarding the importance of the detection of the biomolecule specifies, there are some traditional approaches for the identification of the biomolecules including fluorescent, electrochemical, enzymatic and magnetic[21–23]. Moreover, the biggest weakness of these structures are low sensitivity and labeling process resulting in a high price cost and time-consuming cost. The Ion-Sensitive-Field-Effect-Transistor (ISFET) has been proposed as an efficient way to solve the problem of labeling[24]. Moreover, these biosensors need the buffer solution and does not have ability to detect the neutral biomolecules specifies[24]. Hence, the DM-FET biosensors have been proposed to solve all these concerns. In the current technologies based on DM-FET a nanocavity is created in the gate oxide to trap the biomolecules. Although this approach is interesting, but the biggest problem is the requirement to a high gate oxide thickness for trapping the biomolecules thus reducing the gate control on the channel region[25]. Also, the low biosensing current and low sensitivity are the other weaknesses of traditional DMFET biosensors. The situations will be more critical when the detection of a low concentration of the biomolecules is required. In order to solve these concerns, the work has proposed a novel structure. In this new configuration, the nanocavity is embedded inside the channel region of a junctionless device making sure that a low subthreshold swing, enhanced biosensing current and high sensitivity will be obtained. It is mentioning that the gate oxide thickness can be now safely scaled whit no concern on the sensitivity degradation of the biosensor. Scaling the gate oxide will enable us to apply the proposed biosensor in low-concentration biomolecule detection which is the strength of the proposed biosensor as comparison to other current biosensors. It is worth noting that the proposed biosensor by this novel configuration has given a high ability for achieving high sensing current and high sensitivity.

The biosensors under the study have been designed at 50 nm gate technology. The gate dielectric thickness has been set to 5 nm to have a proper space for the detection of the biomolecule. It is important to note that the limitation on the gate oxide thickness does not exist for the proposed biosensor since the nanocavity is inserted inside the channel region. This has been investigated in the latter parts of the paper. The nanocavity thickness,

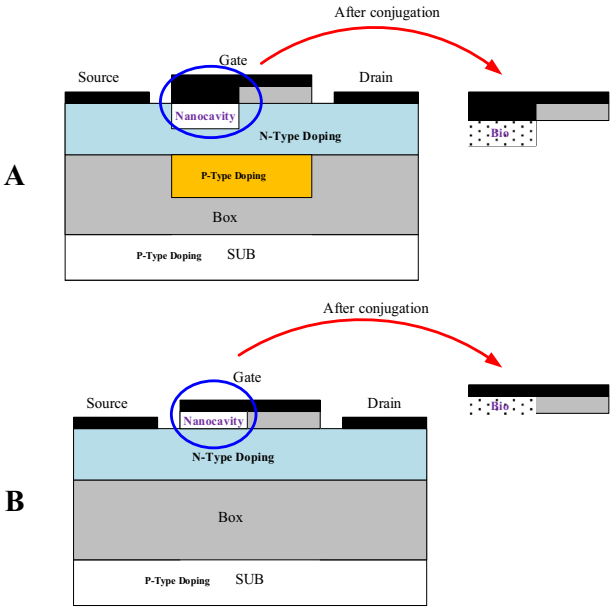

Figure 2. A two-dimensional scheme of (**a**) proposed biosensor, HTRN-JNL and (**b**) conventional biosensor, CJNL implemented in the paper.

nanocavity length, the silicon layer thickness and the buried oxide thickness are the values of 5nm, half to the gate length, 10 nm, and 20 nm, respectively. The silicon layer has been doped at the N-type level of 5×10^{18} cm^{-3}. Also, the gate metal workfunction has been set to 5.1 eV. It is important to state that all the structural parameters of the CJNL biosensor are the same as those of the HTRN-JNL biosensor unless otherwise stated in the paper.

Figure 3 illustrates the suggested steps for the realization of the proposed biodevice originating from a SOI wafer as given in Fig. 3a. Then, a silicon hole trench is created by etching and deposition process according to Fig. 3b. Afterward, a silicon layer with the thickness of 10 nm created by atomic deposition. Also, this step includes the As ion implantation process by the doping concentration of 5e18 cm^{-3} shown in Fig. 3c. Then the etching process is performed to create a via as demonstrated in Fig. 3d. The next step is thermally depositing oxide introduced as a sacrificed layer in order to leave the nanocavity as seen in Fig. 3e[26,27]. It is worth noting that the gate metal is deposited in this step. The next step is a wet etching to leave a via named as the nanocavity inside the channel region according to Fig. 3f including photolithography and etching process. The nanocavity length is controlled by the duration of lateral wet etching with diluted buffered oxide etchant (BOE)[27]. The next step is related to formation of the remining silicon layer including the Si atomic deposition and As ion implantation as illustrated in Fig. 3g. Finally, the source/drain contacts are deposited above the channel region like those performed for the creation of gate electrode in conventional CMOS process[28].

The creation of the hole trench is not a crucial step and is created by an extra lithography mask as compared to the traditional device followed by plasma etching. But, the creation of the nanocavity has a high importance from perspective of the fabrication. The nanocavity is developed by scarifying a SiO_2 oxide layer inserted inside the channel region according to Fig. 3. The nanocavity length is controlled by the duration of lateral wet etching with diluted buffered oxide etchant (BOE). The Buffered oxide etch (BOE), also known as buffered HF or BHF, is a wet etchant used in microfabrication. It is a mixture of a buffering agent such as ammonium fluoride (NH4F), and hydrofluoric acid (HF). Concentrated HF (49% HF in water) etches silicon dioxide too quickly for good process control. Buffered oxide etch is commonly used for more controllable etching in the creation of the nanocavity in the biosensors[20].

Computational scheme

In this section the computational scheme applied in biodevice domain is extensively elucidated. The governing charge transport and Poisson equations are strictly coupled so that extract the drain current. Both the electron and holes are contributed to the simulation domain to reach final drain current for the evaluation of sensing performance.

Beginning with charge transport, the charge continuity law is executed in device domain as following:

$$\frac{\partial n_{(x,y)}}{\partial t} = \frac{1}{q}\nabla\overrightarrow{J_{n\,(x,y)}} + G_{n(x,y)} - R_{n(x,y)} \tag{1}$$

$$\frac{\partial p_{(x,y)}}{\partial t} = -\frac{1}{q}\nabla\overrightarrow{J_{p\,(x,y)}} + G_{p(x,y)} - R_{p(x,y)} \tag{2}$$

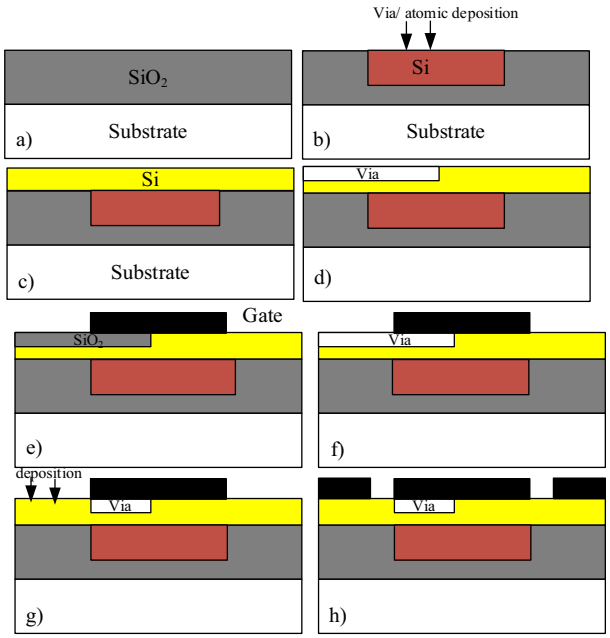

Figure 3. The steps for fabrication of the proposed biosensor.

where x and y in the equations are pointed to the horizontal and vertical directions of device, respectively. The parameters n and p are the electron and hole charge density in the device. The elementary electron charge is introduced by the variable q. The recombination and generation rates of the charges in the cases of R and G are added to the equations. The vectorized important variables $\overrightarrow{J_n}$ and $\overrightarrow{J_p}$ are current density of the charges as given as following:

$$\overrightarrow{J_{n\,(x,y)}} = q\mu_{n(x,y)}\left(-\nabla\psi_{(x,y)} - \frac{\nabla\chi_{e(x,y)}}{q}\right) + D_{n(x,y)}\nabla\left(n_{(x,y)}\right) \tag{3}$$

$$\overrightarrow{J_{p\,(x,y)}} = -q\mu_{p(x,y)}\left(-\nabla\psi_{(x,y)} - \frac{\nabla(\chi_{e(x,y)} + E_{g(x,y)})}{q}\right) + D_{p(x,y)}\nabla\left(p_{(x,y)}\right) \tag{4}$$

According to the relations above $\mu_{n,p}, D_{n,p} = (KT_L/q)\mu_{n,p}$ are the mobility and diffusion constant of both the electron and holes. T and K denote the lattice temperature and Boltzmann constant, respectively. The band-gap energy and the affinity in the relations above are pointed to E_g and χ. For reaching a realistic result, the mobility dependence on the electric field, Klaassen ban-to-band tunneling model and recombination of Shockley–Read–Hall (SRH) are considered the simulation domain[29]. Since our analysis is based on the steady state computations the derivation of n and p with respect to time in Eqs. (1) and (2) must be zero. For solving the charge transport equations, the electrical potential profile should be added to the simulation domain according to the following relation:

$$\nabla\left(\varepsilon_{(x,y)}\nabla\psi\right) = q(n_{(x,y)} - p_{(x,y)} - N_{d(x,y)} + N_{a(x,y)}) - Q_{INT} \tag{5}$$

where ψ is the local electrostatic potential referenced by the intrinsic potential in throughout the simulation domain. ε represents the local permittivity of used materials in the devices. N_d and N_a are donor doping concentration and acceptor doping concentration, respectively. In order to consider issue related to the surface functionality in the proposed device, Q_{INT} as the interface charge is added to Eq. (5). It is worth noting that the fermi static is utilized to model the charge transport since the channel region experiences a high doping density. In Eqs. (1–5) there are some initial parameters can be found in the basic reference[29].

In order to numerically solve the equations, the device space is divided by many grids by horizontal spacing $h_i = x_{i+1} - x_i$ and vertical spacing $K_j = y_{j+1} - y_j$. All the equations should be discretized and computed in these grids. To perform this process, we benefited from the finite box method involving (i − 1, j), (i + 1, j), (i, j − 1) and (i, j + 1) for each (i, j)[30]. This method is based on the integration of the differential equations upon following subdomain:

$$Sub_{i,j} = \left\{x_i - \frac{h_{i-1}}{2} \le x \le x_i + \frac{h_i}{2}, y_j - \frac{K_{j-1}}{2} \le y_j \le y_j + \frac{K_j}{2}\right\} \tag{6}$$

Regarding to the foregoing description, the Poisson equation is converted to the relation bellow by the finite box method as following:

$$\begin{aligned}&\int_{x_i-\frac{h_{i-1}}{2}}^{x_i+\frac{h_i}{2}}\int_{y_j-\frac{K_{j-1}}{2}}^{y_j-\frac{K_j}{2}} \nabla\left(\varepsilon_{(x,y)}\nabla\psi\right)dydx \\ &= \int_{x_i-\frac{h_{i-1}}{2}}^{x_i+\frac{h_i}{2}}\int_{y_j-\frac{K_{j-1}}{2}}^{y_j-\frac{K_j}{2}} q(n_{(x,y)} - p_{(x,y)} - N_{d(x,y)} + N_{a(x,y)})dydx\end{aligned} \tag{7}$$

The charge continuity equations are discretized according to those performed and showed in Eq. (7) as explained in[30,31].

In order to complete the numerical scheme, it is imperative to force the boundary conditions to the device. In the oxide materials in the terms of gate oxide, buried oxide and nanocavity the Poisson equation is only solved whereas both the Poisson and charge transport equations are considered in silicon material and hole trench.

Dirichlet boundary conditions is activated at the ohmic and Schottky contacts. It is pointed out that a fixed potential is assumed at the ohmic contacts containing the source and drain terminals. At Schottky contact which is the either silicon/gate metal interface or oxide/gate metal interface potential is $\psi_G = \chi_{(x,y)} + E_{g(x,y)}/2q + \kappa T_L/2qLn(N_C/N_V) - W_F + V_G$, where where W_F is the workfunction of gate electrode. At the source electrode is the potential is assumed to $\psi_S = (\kappa T_L/q)Ln(N_{D(x,y)}/n_{i(x,y)})$, $n_{(x,y)} = N_{D(x,y)}$, $p_{(x,y)} = n_i^2/N_{D(x,y)}$ and at the drain electrode is assumed to $V = V_D + \psi_S$. The variable V_D is the applied drain voltage with the grounded source terminal.

The Neumann boundary conditions is applied for the semiconductor/vacuum interfaces. It tells us that the electric field and current density along the unit normal vector of the interfaces is zero. The relations are given as the subsequent form:

$$\nabla V.\,\vec{n} = 0, \quad \overrightarrow{J_{n\,(x,y)}}.\,\vec{n} = 0, \quad \overrightarrow{J_{p\,(x,y)}}.\,\vec{n} = 0 \tag{8}$$

Also, in the interface of semiconductor/insulator the equation bellow is defined in order to guarantee the electric flux continuity as given in the following equation:

$$\varepsilon_{Si(x,y)}.\frac{\partial \psi_{(x,y)}}{\partial \vec{n}} - \varepsilon_{oxide(x,y)}.\frac{\partial \psi_{(x,y)}}{\partial \vec{n}} = 0 \tag{9}$$

The oxide in the equation above is attributed to all the oxides and the biomaterials in the nanocavity. In order to solve these equations, the newton algorithm is selected to iteratively solve the equations. The computational scheme can be implemented by the in-house models written by MATLAB software and or the famous simulators such as ATLAS from the SILVACO family included in the work[32]. ATLAS simulator is utilized in this paper in order to evaluate the biodevices. The drift- diffusion simulation model has been used to include the transport physic. To obtain realistic results, several models were activated in the simulation, including Shockley–Read–Hall recombination (SRH model), Auger recombination (Auger model), parallel electric field-dependent mobility (Fldmob model) and band-to-band tunneling (BBT-STD model) accordance with the Eqs. (1–9). The mesh resolution is set to 1 nm. For more accuracy, the mesh resolution in the nanocavity is set to 0.5 nm. The non-cylindrical mesh type by total grid points equal to 15,000 has been considered for the simulation of the biodevices. More details about the proposed biodevice dimension has been listed at Table 1.

To gain realistic results through the simulation, the fundamental equations of ATLAS has been calibrated by experimental data as shown in Fig. 4[7].

Physical mechanism

To solve the problem of scaling issues in thinning the gate oxide and depleting the channel region of the proposed junctionless biosensor, the nanocavity is embedded inside the channel region. Also, for further control of the gate on the channel region the part under the gate electrode just inside the buried oxide is replaced by a hole trench. This reformation of the biosensor makes the redistribution of the energy bands inside the channel region. To support this statement by scientific reasons, the energy profiles along the vertical channel which is 40 nm far away from the device left have been illustrated in Fig. 5 for both the conventional and proposed junctionless biosensors. In this scenario and for better understanding, the nanocavity is empty. According to the figure the carriers inside the channel region for the proposed biosensor are located at a higher energy level with respect to the Fermi energy level. Hence, the energy band of the proposed biosensor obtains more slope as compared to that of the traditional biosensor. Hence, the electric field inside the channel region is formed thus depleting the

Device parameters	HTRN-JNL biodevice
Gate length	50 nm
Gate oxide thickness	5 nm
Nanocavity thickness	5 nm
Nanocavity length	25 nm
Silicon layer thickness	10 nm
Buried oxide thickness	20 nm
N-type channel region doping concentration	5×10^{18} cm^{-3}
Gate electrode workfunction	5.1 eV

Table 1. The proposed biosensor parameters.

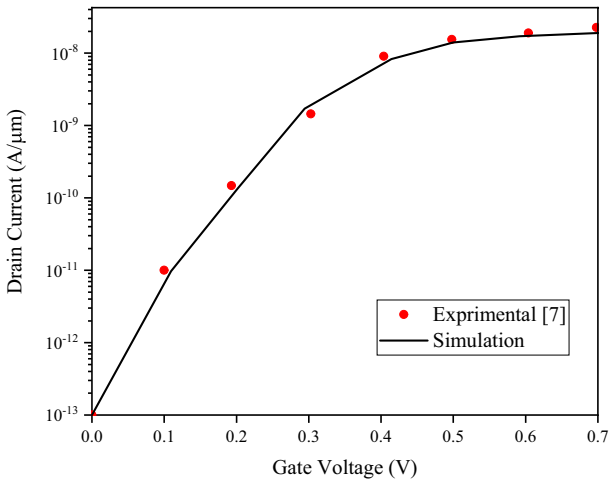

Figure 4. Calibration of the simulator by the experiential data[7].

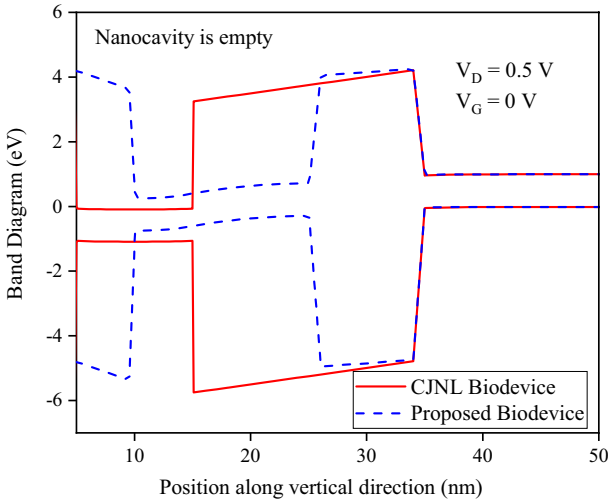

Figure 5. Simulation model calibration against an experimental junctionless data.

channel region. It is worth noting that both the nanocavity and hole trench have an important contribution on the depletion of the channel region in the HTRN-JNL biosensor.

The junctionless structure has been taken into consideration for the nanoscale aims since there is not any gradient on the doping profile making the fabrication scheme easier by suppressing the movement of impurities during the thermal processing. Although this is a profit, but the subthreshold conduction increases, considerably. Since the sensitivity is commonly dependent on the subthreshold region, the functionality of the biomolecule specifies at the nanocavity has a very low impact on the biosensor current due to enhanced subthreshold current. For better perception, the two-dimensional (2D) current densities throughout the HTRN-JNL device, have been depicted as illustrated in Fig. 6. Is it clearly remarked from the figure that only a low area of the channel region of the proposed biosensor participates in current conduction owing to the formation of depletion film caused by the nanocavity and hole trench whereas whole the channel region for the CLNL biosensor is involved in conduction mechanism. Hence, it is expected that the HTRN-JNL biosensor earns a higher dependence on the targeted biomolecules owing to reduced subthreshold swing in comparison to the CLNL biosensor.

Discussion on improvements

The changes in energy band modulation are caused by the biomolecule injection into the nanocavity in both biosensors under the study. To evaluate sensitivity of biosensors, the drain current before and after the injection of the biomolecules should be extracted. Before the injection of biomolecule, the nanocavity is empty and is modeled by the air material by the dielectric constant of $K_{air} = 1$ and after the injection of the biomolecule it is modeled by K_{bio} which is corresponded to the dielectric constant of the related biomolecule. At first, the current sensitivity parameter is calculated according to the equation below:

$$S_{Current} = \frac{I_{d(K_{air})} - I_{d(K_{bio})}}{I_{d(K_{bio})}} \tag{10}$$

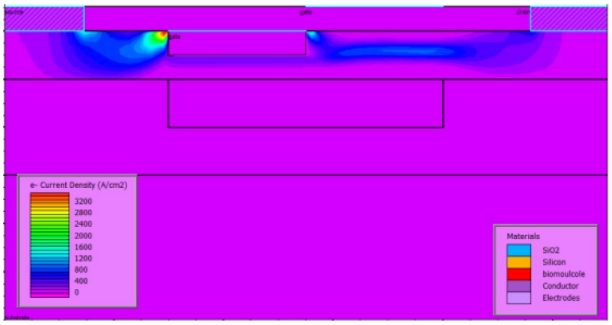

Figure 6. A perspective of two-dimensional (2D) current density for proposed biosensor.

where $I_{d(K_{air})}$ and $I_{d(K_{bio})}$ are the drain current before and after the injection of the biomolecules, respectively. Since relation above has a peak, the biodevice sensitivity is defined as the maximum of current sensitivity in the subsequent form:

$$S_{biosensor} = Max(S_{Current}) \tag{11}$$

In this study, the different types of biomolecules in the cases of Biotin, Protein A, Bacteriophage T7, and Apomyoglobin by dielectric constants ranging from 2 to 8 have been utilized as targeted biomolecules for evaluating the sensitivity of biosensors.

Figure 7 depicts the energy profiles before/after the injection of the Protein A ($K_{bio} = 4$) for the CJNL and proposed biosensors. The figure obviously shows that the energy band diagram is successfully impressed when the Protein A is inserted inside the the nanocavity in the HTRN-JNL biosensor. But, the change in the energy profile of CJNL biosensor is very low and neglectable. Hence, it will be a useful information that the conventional junctionless cannot be considered as an effective biodevice in order to sense the biomolecules.

In order to get a better understanding, the drain current against the gate voltage has been plotted for both the biosensors before/after the injection of the biomolecule in Fig. 8. According to the figure, the proposed biosensor has granted a very reduced subthreshold swing which is an important factor for the enhanced sensitivity of it. Indeed, embedding the nanocavity inside the channel region and the hole trench inside the buried oxide will form a depletion layer to reduce the subthreshold swing. Hence, the drain current of the proposed biosensor is greatly impressed by the different types of the biomolecules thus increasing the sensitivity as compared to the CJNL biosensor.

In order to measure the sensing capability of the proposed biosensor, the current sensitivity upon the gate voltage is plotted in Fig. 9 for both the biosensors. Two biomolecules in terms of Protein A ($K_{bio} = 4$) and

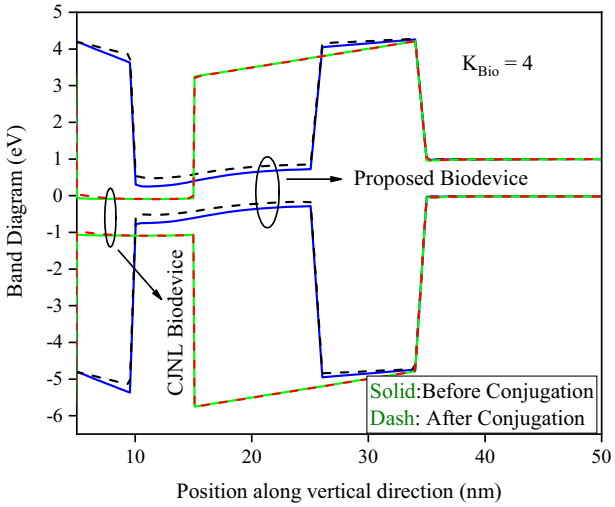

Figure 7. Energy band profiles along the vertical channel for the proposed and conventional biodevice at the conditions of before/after the conjugation of the biomolecule. The Protein A by $K_{bio} = 4$ has been selected as the targeted biomolecule.

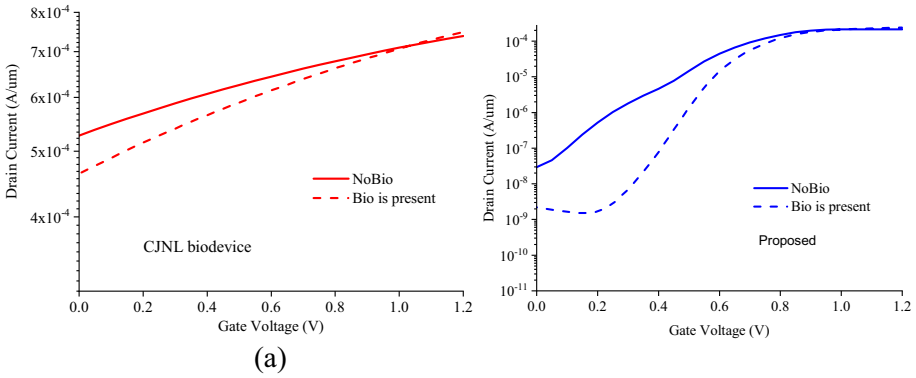

Figure 8. The drain current against the gate voltage for (**a**) the conventional and (**b**) proposed biodevices. The situations in the cases of the absent and present of the biomolecule Protein A have been considered.

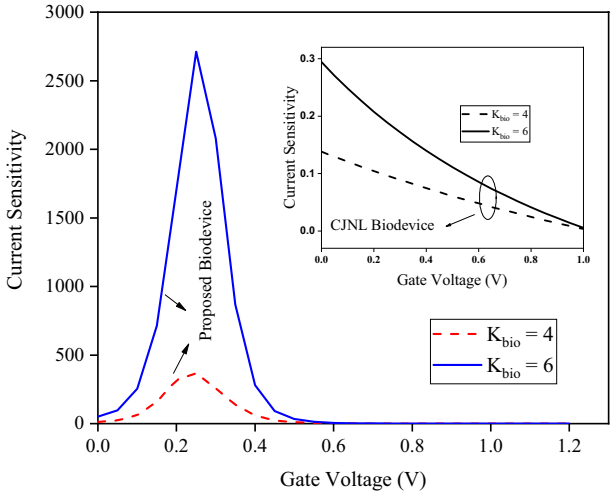

Figure 9. Current sensitivity against the gate voltage for the proposed and conventional biodevices. The biomolecules in terms of Protein A and Bacteriophage T7 have been used for detection.

Bacteriophage T7(K_{bio} = 6) have been included in this investigation. The figure shows the marvelous sensing performance improvement of the proposed biosensor. It is evident from the figure that there is not seen any peak on the curve of sensitivity for the conventional JNL due to enhanced subthreshold swing whereas it is seen for the proposed biodevice. According to the figure, the HTRN-CJNL biosensor gave a much further maximum sensitivity ($S_{biosensor}$) than the CJNL biosensor. It can be expressed that the conventional JNL biosensor is not a suitable candidate for the aims of biosensing. But, by the stated ideas in this work, the junctionless biosensor which is an excellent device in the nanoscale limit can be used as an efficient biosensor by enhanced sensitivity.

The biosensor sensitivity defined according to Eq. (11) is depicted for both the biodevices under the investigation in Fig. 10. Biomolecules in the cases of Biotin, Protein A, Bacteriophage T7, and Apomyoglobin by dielectric constants ranging from 2 to 8 have been utilized as the targeted biomolecules. It can be observed from the figure that the proposed biosensor gives much more sensitivity than the CJNL biosensor. The power of the proposed biosensor is further seen when the dielectric constant increases up to 8. According to the figure and for the biomolecule Apomyoglobin, the proposed biosensor has given an enhanced sensitivity which is 20,000 times more than that for the conventional junctionless biosensor. Therefore, in order to utilize all the benefits of the junctionless device as a biosensor, the junctionless configuration biosensor must be modified according to Fig. 1. The sensing related performance of the suggested biodevice is more highlighted since the sensitivity of the CJNL biodevice is less than 1 for all the biomolecules. It is worth noting that this superiority in sensing performance is owing to the formation of a depletion layer caused by embedded nanocavity inside the channel region and the inserted hole trench inside the buried oxide. A meaningful result is the successful modulation of energy bands to reduce the subthreshold swing thus increasing the variations rate of drain current before/after injection of the biomolecule specifies. It is why the proposed junctionless biosensor has presented a marvelous sensing performance when compared to the CJNL biosensor.

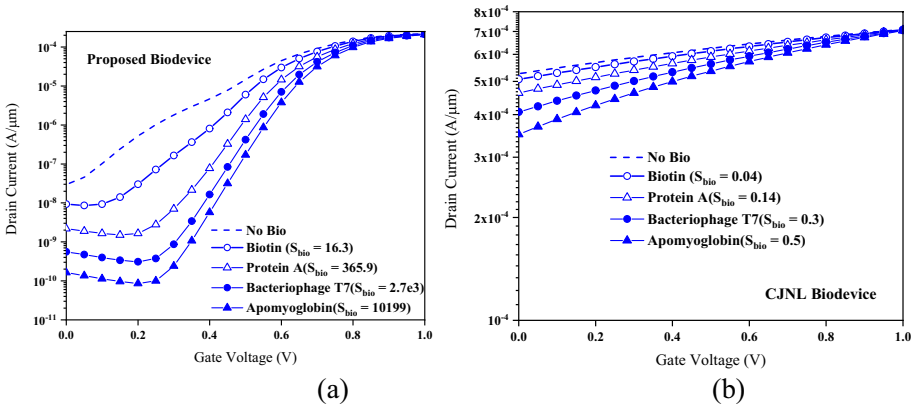

Figure 10. Drain current upon the gate voltage for (**a**) the proposed biosensor and (**b**) the conventional biosensor for the different biomolecules.

The biomolecule hybridized inside the nanocavity can get the negative charges thus changing the sensitivity of the biodevice. For more investigation, the sensitivities of the proposed biosensor for Protein A ($K_{bio} = 4$) by neutral, negative and positive charges have been calculated in Fig. 11. As shown in the figure, for more negative charged biomolecule the decline in the sensitivity of the biosensor is seen. The reason is that the negative charge reduces the depletion layer thickness in the channel region thus increasing subthreshold swing. The conclusion is the reduction of the sensitivity. But, even under this condition, the suggested biodevice has a very great sensitivity as compared to the conventional biosensor. The sensing performance is promoted when the biomolecule is positively charged. For a positive charge, the depletion layer thickness inside the channel region increases resulting in the reduction of the subthreshold swing. The result is the enhancement of the sensitivity of the proposed biosensor.

Designing issues

In this section of the paper, the designing important issues and their roles on the sensitivity of the recommended biodevice are scrutinized. The important factors in terms of the gate oxide thickness, the nanocavity length, and the hole trench are focused in this part. One of the biggest weaknesses of the CJNL biosensor is impossibility of scaling the gate oxide due to limitations on the biomolecule thickness. But, since the nanocavity in the proposed biosensor is embedded inside the channel region the scaling of the gate oxide is possible and can help the proposed biosensor. The drain current against the gate voltage at the different gate oxide thicknesses of 5 nm and 1.2 nm has been plotted for the proposed biosensor in Fig. 12. Focusing on the figure, the subthreshold swing is improved for reduced gate oxide thickness thus reducing the short channel effects which are very desirable at nanoscale applications. Indeed, there is freedom in the proposed biosensor to scale the gate oxide reaching better electric performance as compared to the conventional biosensor.

Figure 13a shows the influence of the gate oxide thickness on the sensitivity of the suggested biodevice. It is seen as an interesting trend on this sensitivity curve. When the gate dielectric thickness is mitigated, the gate coupling on the channel region is enhanced thus decreasing the subthreshold swing. Hence, $I_{d(K_{bio})}$ is reduced resulting in increase in the sensitivity according to Eq. (11). According to the figure the sensitivity reaches the maximum value at the gate oxide thickness of 3.5 nm. By more reduction of the gate oxide thickness after this point, the subthreshold swing is more reduced but since $I_{d(K_{air})}$ is now comparable to $I_{d(K_{bio})}$ then the $(I_{d(K_{air})} - I_{d(K_{bio})})$ becomes so low resulting in decrease in the sensitivity according to Eq. (11). It is important to note that the sensing related performance of the recommended biodevice is still high even for the ultrathin gate oxide when compared to the CJNL biosensor. Also, it can be inferred from the figure that the gate oxide thickness of 3.5 nm is an optimum value to reach the best sensing performance. One of the other important issues in designing the proposed biosensor is related to the nanocavity length. In this scenario, the sensitivity as a function of the nanocavity length has been plotted for the HTRN-JNL biosensor in Fig. 13b.

It is figured out from the figure that the proposed biosensor has still great sensitivity even for reduced nanocavity length of 10 nm which is very favorable for the identification of the biomolecules by low concentration. When the nanocavity length is low, the overlap between the nanocavity and the hole trench is reduced thus increasing the subthreshold swing. Hence, the depletion volume inside the channel region is decreased resulting in enhancement of both $I_{d(K_{air})}$ and $I_{d(K_{bio})}$. Since $(I_{d(K_{air})} - I_{d(K_{bio})})$ is declined the biosensor sensitivity is reduced according to Eq. (11).

The overlap between the nanocavity and hole trench increases terminating in the reduction of the subthreshold swing and in turn the increase in the depletion layer inside the channel region to enhance $(I_{d(K_{air})} - I_{d(K_{bio})})$

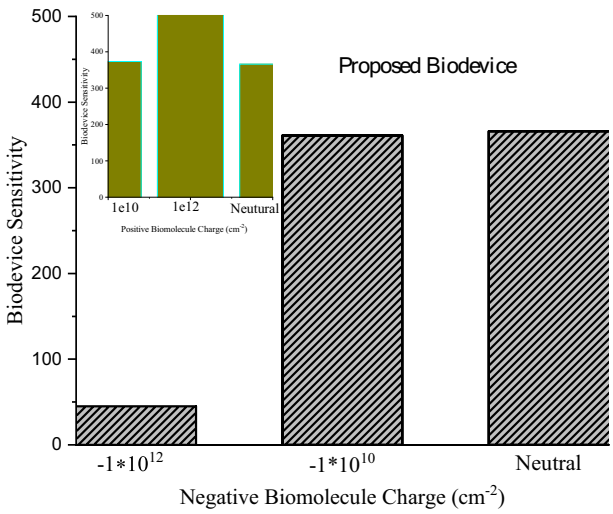

Figure 11. The biomolecule charge impact on the sensitivity of the proposed biosensor. The Protein A by $K_{bio} = 4$ has been selected as the targeted biomolecule. The positive/negative charged biomolecule has different charges.

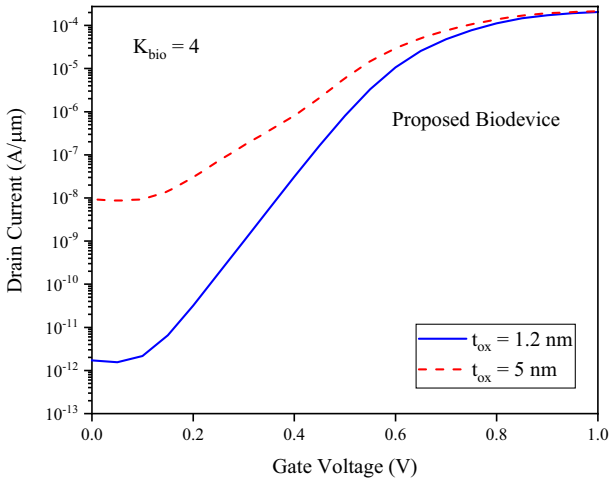

Figure 12. The drain current after conjugation as a function of the gate voltage for the proposed biodevice including the different gate oxides. The Protein A by $K_{bio} = 4$ has been selected as the targeted biomolecule.

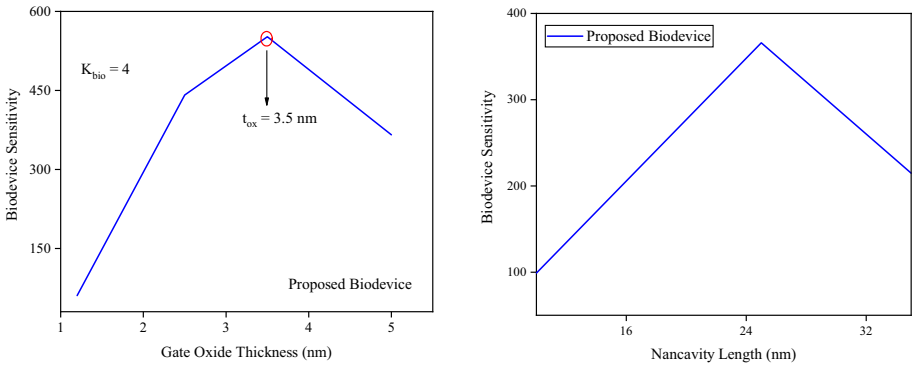

Figure 13. The biodevice sensitivity as a function of and (**a**) gate oxide thickness and (**b**) the nanocavity length for the proposed biosensor. The Protein A by $K_{bio} = 4$ has been selected as the targeted biomolecule.

thus promoting the sensitivity. But, by more increase in the nanocavity length both $I_{d(K_{air})}$ and $I_{d(K_{bio})}$ is considerable enhanced resulting in the reduction of $(I_{d(K_{air})} - I_{d(K_{bio})})$ so the sensitivity is degraded. This is the reason why a maximum point is seen on the sensitivity curve in the figure. Therefore, the nanocavity length of 25 nm which is the half to gate length is selected as the optimum point to attain the best performance on the sensitivity issue.

Not only the proper location of the nanocavity inside the channel region has enhanced the proposed biosensor performance, but also the hole trench plays an important role in the promotion of sensitivity. For this reason, the role of the hole trench on the CJNL and HTRN-JNL biosensors are investigated in the rest. Figure 14 illustrates the role of presence and absence of the hole trench on the sensing performance of the proposed biosensor. The data in the figure clearly show that the sensitivity of the proposed biodevice is exponentially enhanced when the hole trench is present. It is worth noting that the hole trench role of the sensing performance for the CJNL biosensor is also investigated in Fig. 15 for better comparison. It is concluded from the figure that the hole trench has a considerable impact on the sensitivity of the conventional biosensor such that the sensitivity gets values of more than 1. The significance of the proposed biodevice is more exhibited by comparison of Figs. 14 and 15. Regarding to the figure, the proposed biosensor without the hole trench has still a much higher sensitivity than the CJNL biosensor by the presence of the hole trench. It shows that the idea of embedding the nanocavity inside the channel region in the junctionless biosensor is very efficient and recommended especially when the ultra-scaled junctionless biosensor is required.

Technical challenges

Up to now, the ideal conditions have been taken into consideration for the detection of the biomolecule inside the nanocavity. In this section, two main technical issues in the cases of the partial hybridization and the targeted biomolecule's location inside the nanocavity are studied for the proposed biosensor[33].

Biosensor by the absence of the hole trench has still the acceptable sensitivity as compared to the conventional JNL biosensor. It should be noted that the contribution of the hole trench on the sensitivity is more than

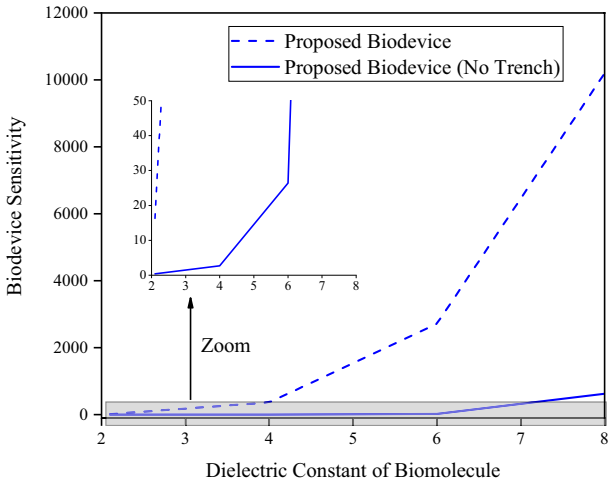

Figure 14. The biodevice sensitivity as a function of the different biomolecules for the proposed biosensor in the conditions of absent and present of the hole trench.

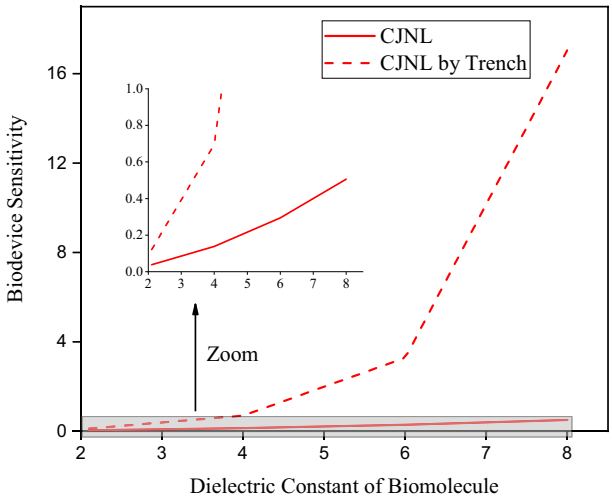

Figure 15. The biodevice sensitivity as a function of the different biomolecules for the conventional biosensor in the conditions of absent and present of the hole trench.

that of the nanocavity. Moreover, the novel location for the nanocavity inside the channel region will enable the proposed biosensor that works in the nanoscale limit by ultrathin gate oxide.

In the experimental conditions it may only a part of the nanocavity is involved in the process of detecting the biomolecules. The figure of merit in the cases of fill-factor defines what the percentage of the nanocavity is occupied by the targeted biomolecules named as the partial hybridization concept. The fill-factor variable is calculated as the relation below:

$$fill - factor = \frac{L_{bio}}{L_{gap}} \tag{12}$$

where L_{bio} is the biomolecule length inside the nanocavity and L_{gap} is the nanocavity length. In order to investigate this practical issue, the fill-factors of 25%, 50%, 75% and 100% have been considered. Protein A ($K_{bio} = 4$) is selected as targeted biomolecule. Figure 16 illustrates the biodevice sensitivity as a function of the fill-factor. It is seen from the figure that the sensitivity is reduced when the fill-factor is reduced. This is because of the reduction of the coupling of the nanocavity on the channel region to mitigate the biomolecule capacitance thus decreasing the biodevice sensitivity. Moreover, the proposed junctionless biosensor has still kept the capability to detect the biomolecule Protein A since the sensitivity value is high. Indeed, in the worst condition i.e. fill-factor of 25% the sensitivity of the recommended biodevice is 25 times more than that of the CJNL biosensor by fill-factor of 100%. Hence, it can be concluded that the HTRN-JNL biosensor is potent to detect low concentrations

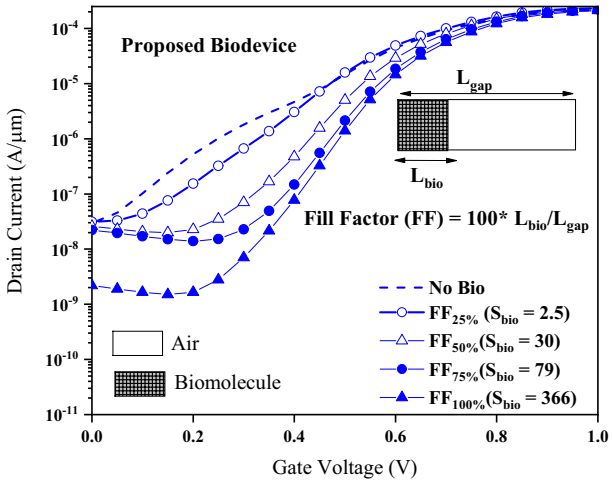

Figure 16. The partial hybridization impact on the sensitivity of the proposed biosensor. The Protein A by $K_{bio} = 4$ has been selected as the targeted biomolecule.

of biomolecules. Hence, the realization of ultra-scale junctionless biosensors involving low density of the biomolecule will be possible.

One of the other technical challenges occurring in the practical conditions is attributed to the targeted biomolecule's location inside the nanocavity. Three different locations for the injected biomolecules in the cases of Case A, Case B, and Case C may occur as shown in Fig. 17. In Case A the biomolecule is located at the nanocavity left side and in Case B it is located at the center and for other one the biomolecule is located at the nanocavity right side. For all three cases only 50% of nanocavity is occupied by the biomolecules. Regarding Case C and according to electric flux continuity, the lateral electric field inside the channel region under the nanocavity is reduced thus decreasing the drain current during the detection of the biomolecule. Hence, the value of $(I_{d(K_{air})} - I_{d(K_{bio})})$ is enhanced to increase the biodevice sensitivity. But for Case A, since the lateral electric field inside the channel region under the nanocavity is increased therefore the drain current is enhanced to reduce $(I_{d(K_{air})} - I_{d(K_{bio})})$. A meaningful result is the reduction of the biodevice sensitivity for Case A. According to Case B, the electric field inside the channel region is first reduced and then increased. Hence, there is tradeoff on the drain current thus preventing more variation of the sensitivity. Then the biodevice sensitivity is nearly equal to the sensitivity in Fig. 16 by the fill-factor of 50%. It is very important to note that for all three cases and according to the obtained biodevice sensitivity, the proposed junctionless biosensor has kept the detection high power of the biomolecule.

One of the important factors to degrade the sensitivity of biosensors is related to the steric hindrance effect induced by the arrangement of biomolecules. Indeed, the biomolecule by a nonuniform distribution is attached to the bioreceptors inside the nanocavity. In order to show this event, two different fill-factors in terms of 50% and 20% has been assumed as illustrated in Table 2. Table 2 shows 4 different cases for the arrangement of the biomolecules. One of the most important result is that the proposed biosensor has still maintained the sensing

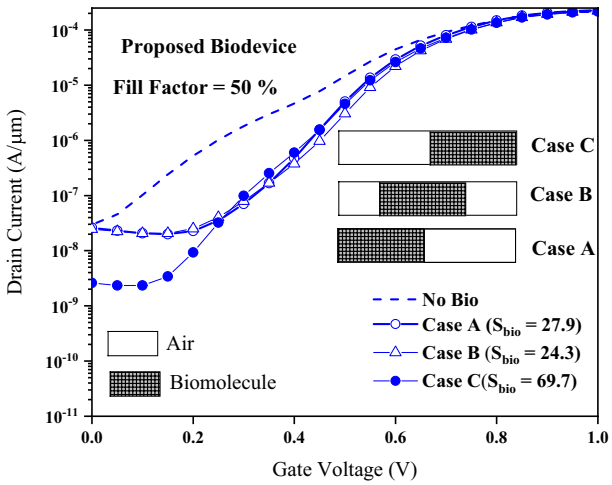

Figure 17. The partial hybridization impact on the sensitivity of the proposed biosensor. The Protein A by $K_{bio} = 4$ has been selected as the targeted biomolecule.

Width of each slot= 2.5 nm, L_g = 50 nm, L_{gap} = 25 nm/ The shaded spaces show the absence of the biomolecule. / Biomolecule sample:		Fill-Factor (%)	S_{bio}
Case 1		50	32
Case 2		50	49
Case 3		20	8.1
Case 4		20	4.2

Table 2. The steric hindrance effect investigation induced by the arrangement of the biomolecules.

performance superiority as compared to the traditional biosensor promising a more reliable biosensor. Cases 1 and 2 are corresponded to the fill-factor of 50%. Case 2 has given a more sensitivity as compared to Case 1. Because the effective channel length controlled by the gate electrode is reduced in Case 2 thus decreasing the drain current. According to the definition of the sensitivity, it is expected that the sensitivity is enhanced as verified in the table. Regarding Cases 3 and 4 related to the fill-factor of 20%, Case 3 has given a more sensitivity as compared to Case 4. Since only a small amount of the nanocavity is filled by the biomolecules, the difference between the drain current before and after the hybridization is the neglectable. Indeed, the channel region experiences a fewer depletion volume. Since the biomolecule in Case 3 is near the source region, the electrostatic coupling on the interface of source/channel is enhanced thus increasing the sensitivity. Moreover, all these cases have given a higher sensitivity as compared to the traditional biosensor promising a biosensor by superior sensing performance.

Comparing with other reports

The proposed biodevice has also given higher sensitivity over the similar biosensors[25,33,34] as demonstrated in Table 3. For proper comparison, the sensitivity is normalized with respect to the nanocavity area filled by the biomolecule. Hence, the normalized sensitivity is defined as following relation:

$$S_{Norm} = \frac{S_{Biosensor}}{Area}, \quad Area = N * (W * T_{gap}) \tag{13}$$

In the equation above, W and T_{gap} are the width and height of the nanocavity, respectively. Also, the parameter N denotes the number of the nanocavity in the biodevice configuration. One of the most advantage of the proposed biosensor is to enable us to scale the gate oxide without the concern on the nanocavity. In the text of the paper it has been shown that for a reduced gate oxide the sensitivity is successfully enhanced giving a S_{Norm} equal to 4.4 nm^{-2} which is much more than other reports.

It is worth noting a SiGe based TFET has been presented in the previously reported work to enhance the sensitivity[33]. Reaching a low subthreshold swing is the most important benefit of the TFET based biosensors. Moreover, the drain current is aggressively reduced by this biosensor impressed adversely by the possible noise in the environment. The aim of the pervious report was to investigate the SiGe role on the enhancement of the sensitivity since it has a lower bandgap and reduced tunneling mass thus increasing the drain current. Although the SiGe can enhance the drain current but the current is still very low for low concentration biomolecules detection. Also, the strain effects induced by the SiGe material along with the low drain currant resulting in the high dependence of the SiGe based TFET on the technological parameters thus degrading the sensitivity. On the other hand, the traditional junctionless based biosensor has a very high drain current and the enhanced subthreshold swing. The high drain current induced by the n-type doped channel region adversely impact on the sensitivity of the biosensor since electron transport is much controlled by the n-type channel region instead of the inserted biomolecules inside the nanocavity. In order to reach a moderate limit between the junctionless biosensor and TFET biosensor, a tradeoff is performed by modification on the traditional junctionless biosnesor architecture. Indeed, the nanocavity is leaded into the channel region to enable us to provide a thinner gate oxide to overcome the short channel effects. Also, by embedding a P-type layer inside the buried oxide a part of the channel region is depleted so that reduce the subthreshold swing and enhance the biosensor sensitivity. All these factors help the proposed biosensor to detect the biomolecules by a higher sensitivity while reducing the degradation.

Biosensor	S_{Norm}	Scaling gate oxide
This work	3.2 nm^{-2}	Yes
[33]	0.6 nm^{-2}	No
[25]	1.6 nm^{-2}	No
[34]	0.5 nm^{-2}	No

Table 3. Comparison of proposed biodevice with other reports.

Setup for immobilization of biomolecule

In order to start the operation of proposed biosensor for the bio-experiments, the proposed biosensor by air nanocavity is cleaned by deionized water (DW) and dried in a high-pressure nitrogen. Afterward the device enters a 1% (v/v) solution of 3-aminopropyltriethoxysilance in ethanol for 30 min. It is rinsed six times and then dried at 120 °C for 10 min. The device is then immersed in a sulpho-NHS-LC-biotin (Pierce) solution for about 1 h[20]. It is worth noting that the Pierce had been previously dissolved in a phosphate-buffered saline solution (PBS, Sigma-Aldrich). After this action, the biotin is reacted at the nanocavity surface. In order to eliminate any unreacted biotins, the biodevice is immediately immersed in a streptavidin/PBS solution for 1 h[20]. Then, the process ends with washing the device by the DW and drying in the nitrogen.

As we know reaching an ideal biosensor by uniform and complete hybridization is impossible due to limitation on the bioreceptors. There are some ways to mitigate this nonideality. One of the main solutions is increasing the selectivity of the biosensor. Proposal of the efficient techniques for the immobilization of biomolecule probes can increase the selectivity. There are a few approaches to immobilize the probe inside the nanocavity. The SAM method is commonly used to immobilize the probes on a solid surface[27,35–37]. Although, this technique is widely used but it needs an extra action to enhance the surface efficiency such as including oxygen plasma and a heating annealing resulting in a getting a biosensor by high selectivity. Also, a new method has been reported to immobilize the biomolecule probes using silica-binding proteins (SBP) which has a strong binding with the SiO2 surface[38]. It has been proved that this new method presents a very high selectivity for the biosensors in comparative to the SAM method. The other solution is to modify the biosensor structure by changing the configuration of it. As shown in the paper, the proposed biosensor by a novel configuration has given a high sensitivity in comparison to the traditional and other biosensors.

Readout circuit of proposed biosensor

Since the drain current as a function of the gate voltage is important to us, it is imperative to consider the readout circuit having capability to measure the drain current for swiped gate voltages, accurately. The proposed technique is to convert the drain current to the voltage and then measure this voltage by a data accusation card. Finally, the drain current will be computed with the help of this voltage. Hence, we need a readout circuit to measure the transfer characteristics of the biosensor. A readout circuit performing this action has been previously proposed in[21] can be utilized as the readout circuit of the proposed biosensor. In Fig. 18 the readout circuit of the proposed biosensor has been shown which is originated from[21]. According to the figure, the drain current from a proposed biosensor is copied by the current mirror technique and the final charges added on CINT. There are some circuit techniques are seen in the circuit to overcome the channel length modulation, power supply and flicker noise. More details have been explained in[21]. After measuring the output voltage by data accusation card, the drain current of the biosensor is computed as the subsequent form:

$$I_D = (V_{OUT} - V_{REF}) \times \frac{C_F}{C_{SH}} \times \frac{C_{INT}}{T_{INT}} \tag{14}$$

where the capacitances in terms of CF, CSH, CINT and integration time of TINT have been presented in[21].

The aim of the presentation of the circuit was to give a circuit for the extracting the drain current. Since the drain current is required to be evaluated and due to the high impact of noise on the current, it is imperative to convert the drain current to the voltage. When the select terminal is tuned at a high voltage level, the circuit starts to work. There is a mirror current source to make a high voltage gain. Also, the buffer operational amplifier is utilized to prevent form the voltage loss. Other circuit elements in the readout circuit are for the noise immunity and stability of the circuit. The extracted voltage is then converted into the drain current and finally the sensitivity is calculated.

Nanocavity thickness impact on sensing performance

It is worth noting that because of the proposed biosensor configuration it is possible to create a higher nanocavity thickness by scarifying a part of the gate electrode placed above the nanocavity. Indeed, the proposed biosensor has a high flexibility in tuning the nanocavity thickness as compared to the traditional biosensors. Also, it is

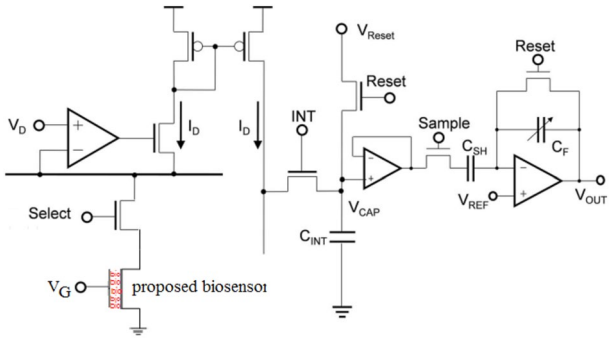

Figure 18. The schematic of readout circuit of the proposed biosensor.

possible to increase the silicon channel thickness to reach a high nanocavity thickness. The nanocavities thicknesses by $t_{gap} = 7$ nm, $t_{gap} = 9$ nm have been investigated to measure the sensing power of the proposed biosensor for considering thicker biomolecules. Figure 19 has illustrated the drain current as a function of the gate voltage for $t_{gap} = 7$ nm, $t_{gap} = 9$ nm. The biomolecule Protein A has been selected for the evaluation of the proposed biosensor. The silicon layer thickness is set to be 11 nm. It is evident from the figure the proposed biosensor has still maintained low subthreshold swing as compared to the traditional biosensor. In order to better understand, the current sensitivity as a function of the gate voltage has been shown in Fig. 20.

It is clearly observed from the figure despite the increasing the biomolecule thickness inside the channel region, the biodevice sensitivity is still much more than that of the traditional biosensor. It is mentioning that the suggested biosensor performance can be promoted by increasing silicon layer thickness and reducing the gate oxide thickness. Since the nanocavity has been created inside the channel region, the proposed biosensor has high flexibility in tuning the sensitivity into an optional situation.

Future research

The aim of the paper is to present a novel biosensor for the detection of the biomolecules. Biotin, Protein A, Bacteriophage T7, and Apomyoglobin have been utilized as targeted biomolecules to evaluate the sensing power of the proposed biosensor. It is worth noting that the performance of the suggested biosensor can be impressed by the different factors which is the interest for the authors in the future research listed in the following:

1. The test of the proposed biosensor on the other biomolecules such avian affluenza and the DNA/RNA strands.

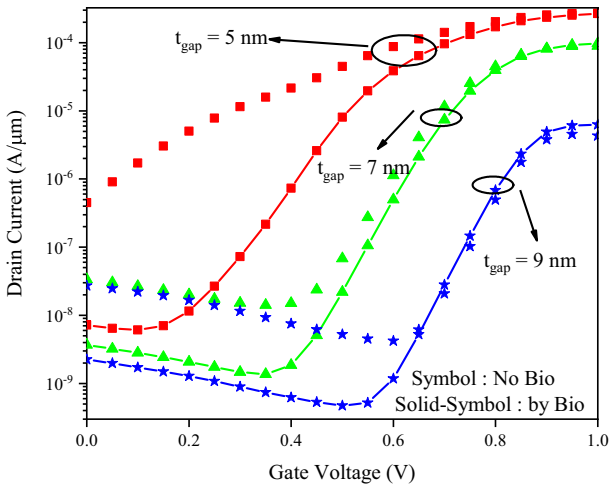

Figure 19. The drain current as a function of the gate voltage for the different nanocavity thicknesses.

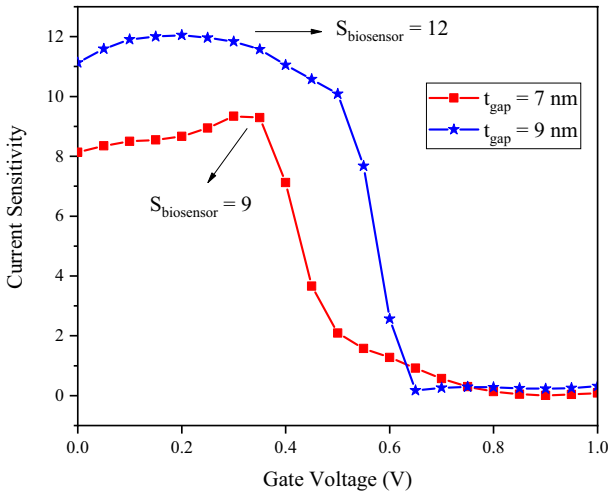

Figure 20. The current sensitivity upon the gate voltage for the different nanocavity thicknesses. The proposed biosensor has still maintained high sensitivity as compared to the traditional device.

2. The optimization of the proposed biosensor including the role investigation of gate length, channel region doping, gate metal workfunction, gate oxide material and the hole trench thickness on the sensing performance.
3. Applying material engineering in the proposed biosensor for the decrease of the steric hindrance induced by the biomolecules.
4. Including the results from control experiments.

Conclusion

For the first time, a new configuration of the junctionless biosensor has been proposed for the enhancement of sensitivity. The nanocavity is appeared at the channel region under the gate oxide. This reformation of the biosensor makes the channel region more depleted thus reducing the subthreshold swing and increasing the sensing related performance. Scaling the gate oxide can be realized in the proposed biosensor unlike the other biosensors. Also, a hole trench is embedded inside the buried oxide to deplete the channel region. A meaningful result is the enhancement of the sensitivity of biodevice. The different types of biomolecules in the cases of Biotin, Protein A, Bacteriophage T7, and Apomyoglobin by dielectric constants ranging from 2 to 8 have been utilized as targeted biomolecules for evaluating sensitivity. The technical challenges related to practical issues including the partial hybridization and targeted biomolecule's location inside the nanocavity have been studied in the proposed biodevice. The obtained results revealed the sensing performance superiority of the proposed biosensor as compared to the conventional biosensor.

Data availability

Availability of data and materials: The datasets used and/or analysed during the current study available from the corresponding author on reasonable request.

Received: 2 March 2024; Accepted: 5 August 2024
Published online: 08 August 2024

References

1. Mehrotra, P. Biosensors and their applications—A review. *J. Oral Biol. Craniofacial Res.* **6**(2), 153–159 (2016).
2. Kumar, A., Tripathi, M. & Chaujar, R. Ultralow-power dielectric-modulated nanogap-embedded sub-20-nm TGRC-MOSFET for biosensing applications. *J. Comput. Electron.* **17**, 1807–1815 (2018).
3. Sadighbayan, D., Hasanzadeh, M. & Ghafar-Zadeh, E. Biosensing based on field-effect transistors (FET): Recent progress and challenges. *TrAC Trends Anal. Chem.* **133**, 116067 (2020).
4. Metkar, S. & Girigoswami, K. Diagnostic biosensors in medicine—A review. *Biocatal. Agric. Biotechnol.* **17**, 271–283 (2019).
5. Narang, R., Saxena, M., Gupta, R. & Gupta, M. Dielectric modulated tunnel field-effect transistor—A biomolecule sensor. *IEEE Electron Device Lett.* **33**(2), 266–268 (2011).
6. Colinge, J.-P. *et al.* Junctionless nanowire transistor (JNT): Properties and design guidelines. *Solid-State Electron.* **65**, 33–37 (2011).
7. Colinge, J.-P. *et al.* Nanowire transistors without junctions. *Nat. Nanotechnol.* **5**(3), 225–229 (2010).
8. Anvarifard, M. K. & Orouji, A. A. Proper electrostatic modulation of electric field in a reliable nano-SOI with a developed channel. *IEEE Trans. Electron Devices* **65**(4), 1653–1657 (2018).
9. Chiang, C.-H. *et al.* Improvements of electrical and thermal characteristics for AlGaN/GaN HEMT grown by metal-organic chemical vapor deposition on silicon-on-insulator (SOI) substrate. *Semicond. Sci. Technol.* **37**(7), 075012 (2022).
10. C.-W. Lee, A. Afzalian, N. D. Akhavan, R. Yan, I. Ferain, and J.-P. Colinge. Junctionless multigate field-effect transistor. *Appl. Phys. Lett.* **94**(5) (2009).
11. Sohrabi-Movahed, A. & Orouji, A. A. Improving specific on-resistance and breakdown voltage in SOI LDMOSs with several N-type windows. *J. Electron. Mater.* **52**(2), 1366–1374 (2023).
12. Mishra, G. S., Mohankumar, N. & Singh, S. K. Impact of InGaN notch on sensitivity in dielectric modulated dual channel GaN MOSHEMT for label-free biosensing. *Curr. Appl. Phys.* **49**, 83–90 (2023).
13. Vu, C.-A. & Chen, W.-Y. Field-effect transistor biosensors for biomedical applications: Recent advances and future prospects. *Sensors* **19**(19), 4214 (2019).
14. Wadhera, T., Kakkar, D., Wadhwa, G. & Raj, B. Recent advances and progress in development of the field effect transistor biosensor: A review. *J. Electron. Mater.* **48**, 7635–7646 (2019).
15. Gundapaneni, S., Ganguly, S. & Kottantharayil, A. Bulk planar junctionless transistor (BPJLT): An attractive device alternative for scaling. *IEEE Electron Device Lett.* **32**(3), 261–263 (2011).
16. Anam, A., Anand, S. & Amin, S. I. Design and performance analysis of tunnel field effect transistor with buried strained Si 1 – x Ge x source structure based biosensor for sensitivity enhancement. *IEEE Sensors J.* **20**(22), 13178–13185 (2020).
17. Anand, S., Singh, A., Amin, S. I. & Thool, A. S. Design and performance analysis of dielectrically modulated doping-less tunnel FET-based label free biosensor. *IEEE Sensors J.* **19**(12), 4369–4374 (2019).
18. Shukla, R. P. *et al.* Planar junctionless field-effect transistor for detecting biomolecular interactions. *Sensors* **22**(15), 5783 (2022).
19. Kumar, N., Dhar, R., Garcia, C. P. & Georgiev, V. P. A novel computational framework for simulations of bio-field effect transistors. *ECS Trans.* **111**(1), 249 (2023).
20. S. Kim, D. Baek, J.-Y. Kim, S.-J. Choi, M.-L. Seol, and Y.-K. Choi. A transistor-based biosensor for the extraction of physical properties from biomolecules. *Appl. Phys. Lett.* **101**(7) (2012).
21. Im, M. *et al.* Development of a point-of-care testing platform with a nanogap-embedded separated double-gate field effect transistor array and its readout system for detection of avian influenza. *IEEE Sensors J.* **11**(2), 351–360 (2010).
22. Kannan, N. & Kumar, M. J. Dielectric-modulated impact-ionization MOS transistor as a label-free biosensor. *IEEE Electron Device Lett.* **34**(12), 1575–1577 (2013).
23. Wu, J. *et al.* DNA-stabilized silver nanoclusters for label-free fluorescence imaging of cell surface glycans and fluorescence guided photothermal therapy. *Anal. Chem.* **90**(24), 14368–14375 (2018).
24. Jakeway, S. C., de Mello, A. J. & Russell, E. L. Miniaturized total analysis systems for biological analysis. *Fresenius' J. Anal. Chem.* **366**, 525–539 (2000).
25. Kanungo, S., Chattopadhyay, S., Gupta, P. S., Sinha, K. & Rahaman, H. Study and analysis of the effects of SiGe source and pocket-doped channel on sensing performance of dielectrically modulated tunnel FET-based biosensors. *IEEE Trans. Electron Devices* **63**(6), 2589–2596 (2016).

26. Im, H., Huang, X.-J., Gu, B. & Choi, Y.-K. A dielectric-modulated field-effect transistor for biosensing. *Nat. Nanotechnol.* **2**(7), 430–434 (2007).
27. Kim, C.-H., Jung, C., Lee, K.-B., Park, H. G. & Choi, Y.-K. Label-free DNA detection with a nanogap embedded complementary metal oxide semiconductor. *Nanotechnology* **22**(13), 135502 (2011).
28. Ramezani, Z. & Orouji, A. A. A novel double gate MOSFET by symmetrical insulator packets with improved short channel effects. *Int. J. Electron.* **105**(3), 361–374 (2018).
29. S.M. Sze, Kwok. K. Ng. *Physics of Semiconductor Devices*, 3rd edn. (Wiley, 2006.)
30. R.S .Varga. *Matrix Iterative Analysis* (Prentice-Hall, 1962).
31. S. Selberherr. Analysis and Simulation of Semiconductor Devices, Springer; Softcover reprint of the original 1st ed. (1984).
32. S. C. SILVACO ATLAS Device Simulation Software, CA, USA, and O. A. https://silvaco.com.
33. Anvarifard, M. K., Ramezani, Z., Amiri, I., Tamersit, K. & Nejad, A. M. Profound analysis on sensing performance of Nanogap SiGe source DM-TFET biosensor. *J. Mater. Sci. Mater. Electron.* **31**, 22699–22712 (2020).
34. Lodhi, A. *et al.* Sensitivity and sensing speed analysis of extended nano-cavity and source over electrode in Si/SiGe based TFET biosensor. *Appl. Phys. A* **126**(11), 837 (2020).
35. Anvarifard, M. K., Ramezani, Z. & Amiri, I. S. Label-free detection of DNA by a dielectric modulated armchair-graphene nanoribbon FET based biosensor in a dual-nanogap setup. *Mater. Sci. Eng. C* **117**, 111293 (2020).
36. Kim, C.-H., Jung, C., Park, H. G. & Choi, Y.-K. Novel dielectric modulated field-effect transistor for label-free DNA detection. *Biochip. J.* **2**(2), 127–134 (2008).
37. Poghossian, A., Cherstvy, A., Ingebrandt, S., Offenhäusser, A. & Schöning, M. J. Possibilities and limitations of label-free detection of DNA hybridization with field-effect-based devices. *Sensors Actuators B Chem.* **111**, 470–480 (2005).
38. Gu, B. *et al.* Nanogap field-effect transistor biosensors for electrical detection of avian influenza. *Small.* **5**(21), 2407–2412 (2009).

Author contributions

M. K.Anvarifard: Conceptualization, Writing -original draft, Software. Ali A. Orouji: Investigation, review & editing. All authors reviewed the manuscript.

Competing interests

The authors declare no competing interests.

Additional information

Correspondence and requests for materials should be addressed to M.K.A.

Reprints and permissions information is available at www.nature.com/reprints.

Publisher's note Springer Nature remains neutral with regard to jurisdictional claims in published maps and institutional affiliations.